Polarized Raman study of NO_2^- in KCl, KBr, KI, and NaBr

Hilde Fleurent*
Physics Department, University of Antwerp (Universitaire Instelling Antwerpen), B-2610 Wilrijk (Antwerpen), Belgium

Wim Joosen
Foundation for Fundamental Research on Matter (FOM), Institute for Atomic and Molecular Physics, Stichting voor Fundamenteel Onderzoek der Materie Kruislaan 407, NL-1098 SJ Amsterdam, The Netherlands

Dirk Schoemaker
Physics Department, University of Antwerp (Universitaire Instelling Antwerpen), B-2610 Wilrijk (Antwerpen), Belgium

(Received 20 July 1989; revised manuscript received 7 November 1989)

The NO_2^--molecular impurity is shown to exhibit different equilibrium orientations depending on the alkali-halide host lattice. The polarized Raman intensities of the three internal modes reflect a twofold axis for the NO_2^- ion in KI and NaBr and a threefold axis in KCl and KBr. For KCl and KBr the quasifree rotation of the molecule around the O—O axis is responsible for the axial behavior of the derived polarizability tensor. The Raman-active gap mode in KI is identified as an A_2 mode of the C_{2v} point group. This mode involves as such a purely rotational motion of the impurity around its dipole axis and is therefore different from the three ir gap modes. The 60-cm^{-1} mode in KI is shown to possess A_1 character and this necessitates a reconsideration of the fine structure of the $\nu_1(A_1)$ mode (1308 cm^{-1}), previously explained as a Fermi resonance between the combination mode of this 60-cm^{-1} mode with the asymmetric-stretching mode and the totally-symmetric-stretching mode. In relatively highly doped crystals (>1 mol %), different and new polarized Raman properties are detected, revealing symmetry lowering and preferential orientation.

I. INTRODUCTION

A large number of spectroscopic techniques has been used to investigate the complex dynamics of the NO_2^- ion, when substituted for a halide ion in the alkali halides. The NO_2^- impurity is a triatomic, bent C_{2v} point-group-symmetry molecule with an intrinsic electric dipole moment of about 0.2 D along the twofold axis.[1] Three normal modes can be distinguished: the symmetric-stretching mode $\nu_1(A_1)$, the symmetric-bending mode $\nu_2(A_1)$, and the asymmetric-stretching mode $\nu_3(B_1)$. As such the vibrational spectra of this molecular ion can be separated into (a) a high-frequency region with the internal vibrational modes (>700 cm^{-1}), which show relatively small frequency changes depending on the host lattice, and (b) a low-frequency region (0–300 cm^{-1}), which reveals the perturbation of the pure lattice by the impurity ion. Very specific information about these spectral regions was retrieved from infrared[2] (ir) and far-infrared (FIR) absorption[3–6] and from uv electronic absorption[7–9] and emission.[7,9] Raman measurements were performed to complement this information.[8,10–14]

The data relevant for this paper are summarized below. For the determination of the site symmetry of the NO_2^- in KCl and KBr, the technique of electric-field-induced alignment was used.[2] At 2 K no effect was registered on the ir absorption of the internal modes, so that a reorientational motion of the molecules down to very low temperatures was suggested. The sideband structure in the ir and vibronic spectra revealed an almost free one-dimensional rotation of the ion around the O—O axis.[2,9,14] In KI, these sideband features are different. They were interpreted as being due to hindered rotational motions around all axes. The splitting pattern of the high-frequency ir absorption spectrum in KCl upon application of uniaxial stress was found to be compatible with a $\langle 110 \rangle$ orientation of the dipole axis.[2] These stress measurements were only performed for KCl, but the results were tentatively generalized to all other alkali halides. Recent ir spectral holeburning experiments in the $\nu_2(A_1)$ bending mode of the NO_2^- in KI revealed a $\langle 100 \rangle$ direction of the dipole axis.[5,15] The splitting of the totally-symmetric $\nu_1(A_1)$ Raman mode at 1308 cm^{-1} in KI was explained as a Fermi resonance between the combination mode $\nu_3(B_1)+\nu'$ and $\nu_1(A_1)$, in which ν' was associated with the low-frequency Raman mode at 60 cm^{-1} (Ref. 11).

The low-frequency gap region in KI, which extends from 69.7 to 95.6 cm^{-1} (Ref. 16), turned out to be one of the most interesting features of the NO_2^- system. The complete orthogonality between the Raman scattering and FIR absorption results, which is not expected according to the selection rules of the C_{2v} point group, has been tentatively approached from theoretical[8,17] and experimental[5,6,8] viewpoints.

This paper reports on polarized Raman measurements of the high-frequency region for NO_2^- in KCl and KBr and of both the high- and low-frequency regions for NO_2^- in KI and NaBr. In Sec. III the Raman spectra are presented and the intensity parameters s/q and r/q, extracted from the polarized Raman intensities, are tabulated. A behavior-type analysis[18] of the intensity parameters of the internal vibrational modes reveals different symmetries for the NO_2^- in KI and NaBr (C_{2v}) and in KCl and KBr (C_{3v}), as is shown explicitly in Sec. IV. These data also reflect the quasifree one-dimensional rotation of the ion around the O—O axis in KCl and KBr. In Sec. V new and specific characteristics of the polarized intensities in highly nitrite doped (>1 mol %) crystals are reported. The gap region (Sec. VI) and the Fermi resonance at 1308 cm^{-1} in KI (Sec. VII) are discussed in separate sections.

II. EXPERIMENTAL DETAILS

The KI samples were doped with 0.03 and 1.8 mol % of KNO_2. For KBr 0.05 and 1.4 mol % KNO_2-doped samples were used. The KCl and NaBr samples contained 1.4 and 1.5 mol % of KNO_2 and $NaNO_2$, respectively. The crystals were tightened on a small copper plate in a cold-finger-type cryostate (Cryogenics Associates). The temperature readout was done with a calibrated Si diode in the bottom of the cold finger (i.e., a homogeneous copper block), at ± 1 cm from the sample, yielding an accuracy of 0.2 K.

The polarized Raman spectra were excited with the 514.5- and 488.0-nm laser lines in the commonly used perpendicular scattering setup.[19] The well-known polarization geometries $\langle 110\rangle\langle 1\bar{1}0\rangle$, $\langle 1\bar{1}0\rangle\langle 1\bar{1}0\rangle$, and $\langle 1\bar{1}0\rangle\langle 001\rangle$ can be retrieved from Ref. 18 [OGP set 3, Fig. 2(c)], in which the polarization directions of the incident and detected scattered light are denoted as $\langle\alpha\rangle$ and $\langle\beta\rangle$, respectively. The corresponding scattered intensities $I_{\alpha\beta}$ are indicated as $I_{xy,x\bar{y}}$, $I_{x\bar{y},x\bar{y}}$, and $I_{x\bar{y},z}$.

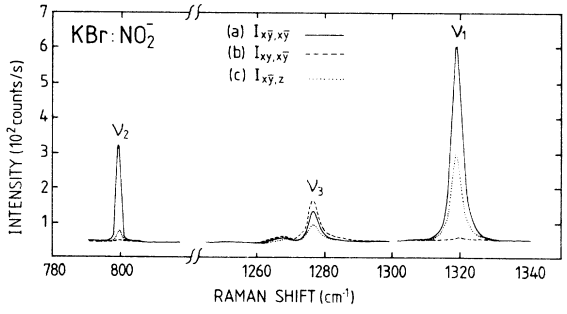

FIG. 1. Polarized Raman spectra of $KBr:NO_2^-$ under 514.5-nm excitation. The data for $\nu_1(A_1)$ and $\nu_2(A_1)$ were recorded in a 0.05 mol % KNO_2-doped sample (900 mW, $T=20$ K). The lower optical quality of the {110}-polished 0.05 mol % doped sample, reducing the signal-to-noise ratio, forced us to increase the light power (900 mW). This enhanced the recording temperature to 20 K and induced a strong broadening of the $\nu_3(B_1)$ mode, inhibiting accurate intensity measurements. Therefore the ν_3 intensities were measured in a 1.4 mol % KNO_2-doped sample (240 mW, $T=14$ K) and rescaled to the 0.05 mol % doped sample by comparing the $\nu_1(A_1)$ data for both concentrations. For presentational purposes the ν_3 intensities have been multiplied by 4.

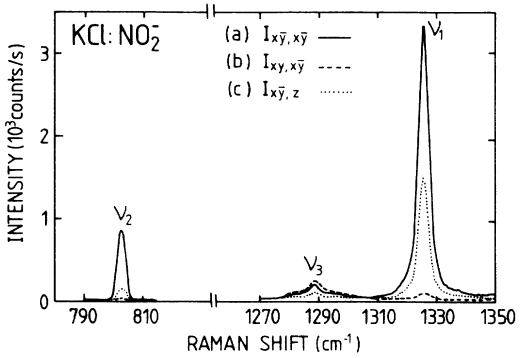

FIG. 2. Polarized Raman spectra of KCl:1.5 mol % KNO_2 under 514.5-nm excitation (300 mW, $T=13$ K).

III. POLARIZED RAMAN SPECTRA

The Raman data $I_{x\bar{y},x\bar{y}}$, $I_{xy,x\bar{y}}$, $I_{x\bar{y},z}$ of the internal modes of the NO_2^- in KBr, KCl, and KI are presented in Figs. 1–3. For the NaBr crystal, which is—due to its hygroscopic properties—difficult to polish without considerable loss of optical transparency, only Raman measurements on a {100}-cut sample were performed. The spectra I_{yy} and I_{yz} of the internal modes of $NaBr:NO_2^-$ are shown in Fig. 4. The Raman data of the low-frequency region of $Kl:NO_2^-$ and $NaBr:NO_2^-$ are presented in Figs. 5 and 6, respectively.

These polarized Raman data were analyzed with the behavior-type (BT) analysis for randomly oriented defects,[18] which allows one to deduce to the largest possible extent the point group of the defect and the irreducible representation of the mode under study. The analysis is based on the values of the intensity parameters s/q and r/q, which can be deduced from the intensities $I_{\alpha\beta}$. The s/q and r/q ratios contain the elements of the Raman tensor, the form of which is group-theoretically determined for each point group and its irreducible representations. In Table I the s/q and r/q ratios of the dynamical modes of NO_2^- in different alkali halides are listed, as

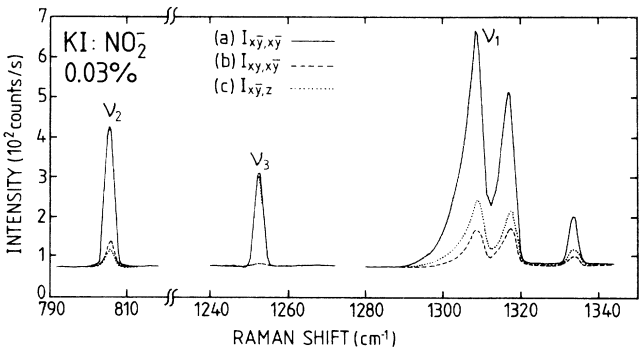

FIG. 3. Polarized Raman spectra of KI:0.03 mol % KNO_2 under 488.0-nm excitation (600 mW, $T=13$ K).

TABLE I. Peak positions ν in cm^{-1} and intensity parameter ratios s/q and r/q for the internal modes $\nu_1(A_1)$, $\nu_2(A_1)$, and $\nu_3(B_1)$ of NO_2^- in KBr, KCl, KI, and NaBr, as derived from the polarized Raman intensities $I_{\alpha\beta}$ in Figs. 1–4. Similar data for the low-frequency ($\leq\omega_{LO}$) modes ν', ν'', and ν''' in KI and NaBr (Figs. 5 and 6) are presented in the lower part of the table. The s/q and r/q ratios for the $\nu_3(B_1)$ mode in KCl have been obtained by fitting the internal mode and both sidebands (see Fig. 2) with Lorentzians, which explains the larger error bars.

	ν (cm^{-1})[a]			s/q	r/q	s/q	r/q	s/q	r/q
	$\nu_1(A_1)$	$\nu_2(A_1)$	$\nu_3(B_1)$	$\nu_1(A_1)$		$\nu_2(A_1)$		$\nu_3(B_1)$	
KBr	1317	799	1276	0.80±0.06	0.97±0.08	0.13±0.03	0.99±0.08	0.30±0.03	−0.48±0.06
KCl	1325	800	1288	0.72±0.04	0.95±0.06	0.19±0.02	0.95±0.06	0.28±0.10	−0.41±0.10
KI	1308	804.5	1252	0.34±0.03	0.63±0.05	0.11±0.03	0.67±0.06	0.00±0.02[b]	0/0[c]
NaBr	1327	827	1278.5	0.31±0.05	d	0.19±0.04	d	0.00±0.03[b]	d
	ν'	ν''[e]	ν'''	ν'		ν''		ν'''	
KI	60	78.8	138	2.60±0.40	0.07±0.15	0.01±0.02	−0.50±0.04	0.00±0.03	−0.97±0.08
NaBr		113				0.00±0.03	d		

[a]Accuracy ±1.5 cm^{-1}, except for ν'' in KI:NO_2^- (0.5 cm^{-1}).
[b]The ratio q/s is indicated. This case corresponds to $q=0$ and $s>0$ within experimental error.
[c] 0/0 indicates $r=0$ and $q=0$ within experimental error.
[d]Only available from {110}-polished samples.
[e]Gap modes.

calculated from the polarized Raman intensities of Figs. 1–6. These results are discussed in Sec. IV.

The influence of the NO_2^- concentration on the polarized Raman intensities was investigated for KI doped with 0.03 and 1.8 mol% KNO_2 and KBr, containing 0.05 and 1.4 mol% KNO_2. Raman spectra for the KI:NO_2^- samples are presented in Figs. 3 and 7. The differences, listed in Table II, are remarkable and new and will be discussed in Sec. V.

IV. SYMMETRY DETERMINATION

A. Previous symmetry assignments

From 1966 onwards it has been generally assumed that in all alkali halides the NO_2^- is distributed among 12 equivalent equilibrium orientations, in which the dipole axis is pointing along a ⟨110⟩ direction, (i.e., point group C_{2v}). This was established by considering the effects of uniaxial stress on the ir absorption of the $\nu_1(A_1)$ and $\nu_3(B_1)$ mode in KCl.[2] The interpretation of the uv dichroism in KI, KCl, and KBr led, erroneously as will be shown in this paper, to the conclusion that the O—O axis lies along ⟨100⟩.[8] Most of the later theoretical and experimental work was based on this site symmetry. Very recently, Ambrose and Sievers obtained contradicting results by persistent ir spectral holeburning in the $\nu_2(A_1)$ bending mode of the NO_2^- in KI: The NO_2^- possesses indeed a C_{2v} point group, but with a ⟨100⟩ directed dipole axis and a {110} molecular plane.[5]

B. Polarized Raman scattering of the NO_2^- internal modes

The polarized Raman data of the internal modes of a molecular impurity in a cubic lattice reflect its site symmetry. It was shown that proper analysis of these Raman data with the BT method for randomly oriented defects[18] provides a dependable method for deducing the equilibrium orientations of linear diatomic[20] and triatomic[21] molecules.

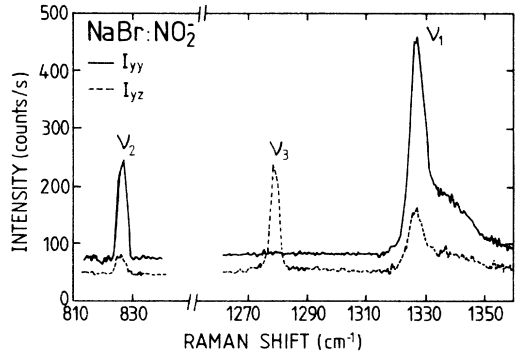

FIG. 4. Polarized Raman spectra of a {100}-cut NaBr:1.5 mol% $NaNO_2$ sample under 514.5-nm excitation (450 mW, $T=11$ K).

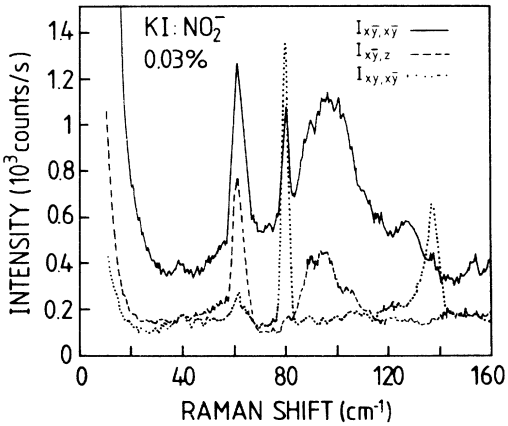

FIG. 5. Polarized Raman spectra of KI:0.03 mol% KNO_2 under 488.0-nm excitation (600 mW, $T=13$ K).

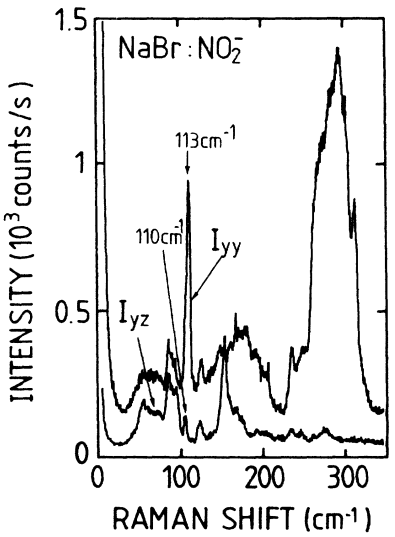

FIG. 6. Polarized Raman spectra of a {100}-cut NaBr:1.5 mol % $NaNO_2$ under 514.5-nm excitation (450 mW, $T=11$ K).

The Raman spectra of the internal modes of NO_2^- in the different alkali halides (Figs. 1–4) reveal a different polarized Raman behavior in the various optical geometries. The BT intensity parameters s/q and r/q (Table I) underline quantitatively the differences between the NO_2^- molecules in the different crystals. A separation into two subgroups with (a) KI and NaBr, and (b) KCl and KBr is justified.

1. KI and NaBr

Following the Zhou-Goovaerts-Schoemaker BT nomenclature,[18] we deduce for Ki and NaBr, using the s/q and r/q ratios of Table I, a BT 60 and a BT 15 for the A_1 and B_1 internal modes, respectively. The symmetry group consistent with both observed BT's is characterized by a twofold axis (see Table VIII of Ref. 18).

Depending on the orientation of the dipole axis and the O—O axis, four possible C_{2v} geometries for the NO_2^- can be distinguished. The possibilities, in which the electric dipole moment and the O—O axis are both lying along ⟨110⟩ directions or along ⟨100⟩ directions, can be eliminated. The first situation requires a BT 14 for the B_1 mode, the second a BT 50 for the A_1 mode. This does not correspond with the experimental data. The two other cases, in which the dipole axis is oriented along a ⟨110⟩ direction and the O—O axis along a ⟨100⟩ direction and vice versa, cannot be discriminated by a BT analysis of A_1 and B_1 modes only. Both cases are actually compatible with the Raman data and this was not recognized in previous Raman investigations.[10,11]

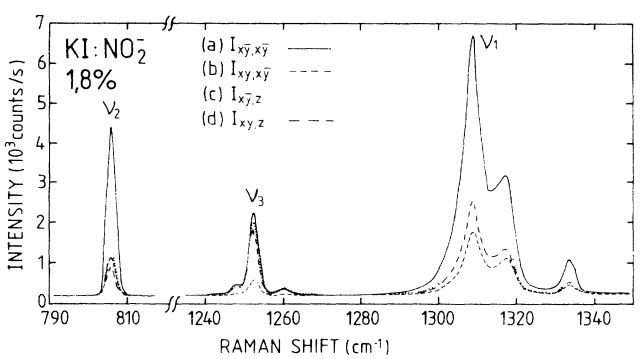

FIG. 7. Polarized Raman spectra of KI:1.8 mol % KNO_2 under 514.5-nm excitation (240 mW, $T=14$ K).

The holeburning experiments have shown that the dipole axis of the NO_2^- in KI is ⟨100⟩ oriented and the molecular plane coincides with a {110} plane.[5] As such our polarized Raman analysis is consistent with these results.

The few experimental data available for NaBr:NO_2^-, such as Raman[8] and uv absorption measurements,[7,8] did not show any pronounced differences with those of the other host lattices. Therefore one agreed up until now upon the generally assumed ⟨110⟩ orientation of the dipole axis. From our Raman investigations on a {100}-cut sample (Fig. 4), we deduce for the internal modes of the NO_2^- in NaBr similar s/q ratios (Table I) as for KI:NO_2^-. In particular, the $q=0$ value for the $\nu_3(B_1)$ mode, characterizing BT 15, allows one to establish the parallellism with KI:NO_2^- without the explicit determination of the r/q ratio. Therefore the NO_2^- in NaBr probably possesses the same site symmetry as in KI.

2. KCl and KBr

The Raman spectra of the A_1 and B_1 internal modes of NO_2^- in KBr and KCl (Figs. 1 and 2) yield s/q and r/q ratios (see Table I), corresponding to a BT 39 and a BT 40, respectively. For randomly oriented defects the combination of these BT's corresponds to a point group with a threefold axis (see Table VIII of Ref. 18). This result is unexpected because of the intrinsic twofold axis of the free NO_2^- ion and suggests an axial behavior of the NO_2^- in KCl and KBr. Similar polarized Raman intensities were also detected for the linear NCO^- in KBr, the molecular axis of which is lying along a ⟨111⟩ direction.[21]

The polarized Raman intensities, corresponding to different orientations of the dipole and O—O axes in the cubic lattice, can be calculated, starting from the A_1 and B_1 Raman tensors of the free species.[22] The diagonal A_1 tensor of the C_{2v} point group is characterized by the nonzero tensor elements xx, yy, and zz, the B_1 mode by the nonzero off-diagonal xz components. The detected polarized Raman intensities for the B_1 mode can only be reproduced when either the dipole axis or the O—O axis are oriented along a ⟨111⟩ direction. The rotational motion around the ⟨111⟩ axis of the oxygen in the first case and the nitrogen in the second case can be characterized by the rotation angle α. The elements of the Raman tensor depend on α, but the polarized Raman intensities, which depend quadratically on these tensor elements, do not. The zero $I_{xy,x\bar{y}}$ intensity for the A_1 mode is only found if $xx=yy$ or $yy=zz$, respectively, which corresponds to *axial* behavior around the [111] direction. The orthorhombic structure of the NO_2^-, which requires three different diagonal elements, is very hard to recon-

TABLE II. Concentration effects in the polarized Raman intensities $I_{\alpha\beta}$ of KI doped with 0.03 and 1.8 mol % KNO_2 and KBr containing 0.5 and 1.4 mol % KNO_2. For KI:NO_2^- and KBr:NO_2^- results for the internal modes $\nu_1(A_1)$ and $\nu_2(A_1)$ are presented. For KI:NO_2^- also the $\nu_3(B_1)$ and the low-frequency modes ν', ν'', and ν''' are compared. Error bars are mainly determined by photon counting statistics and small misalignments of the crystal with respect to the laser beam. For all samples, independent of concentration, the relation $I_{xz}/I_{yz}=1$ was retrieved.

	$\nu_1(A_1)$	$\nu_2(A_1)$	$\nu_3(B_1)$	$\nu_1(A_1)$	$\nu_2(A_1)$	$\nu_3(B_1)$
KI		0.03% KNO_2			1.8% KNO_2	
I_{xz}/I_{xy}	0.97±0.04	0.97±0.12	1.02±0.04	0.86±0.02	0.48±0.02	1.13±0.02
I_{yz}/I_{yy}	0.36±0.03	0.11±0.03	0.00±0.02[a]	0.43±0.02	0.12±0.02	0.15±0.02[a]
$I_{xy,z}/I_{x\bar{y},z}$	0.97±0.07	1.00±0.10	1.00±0.06	0.88±0.03	0.65±0.03	0.92±0.03
$I_{xy,x\bar{y}}/I_{x\bar{y},x\bar{y}}$	0.16±0.02	0.17±0.03	0.00±0.03	0.24±0.02	0.22±0.02	0.20±0.02
KBr		0.05% KNO_2			1.4% KNO_2	
$I_{xy,z}/I_{x\bar{y},z}$	1.00±0.05	1.00±0.10		0.80±0.02	0.74±0.07	
$I_{xy,x\bar{y}}/I_{x\bar{y},x\bar{y}}$	0.01±0.02	0.00±0.02		0.05±0.02	0.03±0.02	
	ν'	ν''	ν'''	ν'	ν''	ν'''
KI		0.03% KNO_2			1.8% KNO_2	
I_{xz}/I_{xy}[b]	0.92±0.10	0/0	0/0	1.08±0.03	0.26±0.05	1.30±0.10
I_{yz}/I_{yy}	0.38±0.06[a]	0.01±0.02	0.00±0.03	0.30±0.05[a]	0.04±0.01	0.06±0.02
$I_{xy,z}/I_{x\bar{y},z}$[b]	0.99±0.04	0/0	0/0	0.95±0.10	0.62±0.03	0.69±0.10
$I_{xy,x\bar{y}}/I_{x\bar{y},x\bar{y}}$	0.15±0.03	0.35±0.03[c]	0.01±0.04[c]	0.29±0.05	0.42±0.03[c]	0.55±0.10[c]

[a]The ratio I_{yy}/I_{yz} is indicated.

[b]0/0 indicates a ratio of intensities, which are zero within experimental accuracy.

[c]The ratio $I_{x\bar{y},x\bar{y}}/I_{xy,x\bar{y}}$ is indicated.

cile with such "accidental" relations. The detected polarized Raman intensities therefore are not compatible with a static NO_2^-.

C. Dynamical behavior

Different dynamics of the NO_2^- depending on the host lattice were demonstrated by low-temperature ac dielectric measurements.[1] These indicated that in KCl and KBr the NO_2^- dipoles were reorienting down to 1 K, while in KI a barrier for reorientation of about 115 cm^{-1} and an off-center position of the center of charge were observed. In KCl and KBr the rotational fine structure on the ir absorption of the $\nu_1(A_1)$ and $\nu_2(A_1)$ modes revealed an almost free rotation of the ion around the O—O axis,[2] for which additional evidence was retrieved from the rotational fine structure of the vibronic absorption and luminescence spectra.[2] The different characteristics of the KI spectra were interpreted in terms of considerably higher potential barriers and hindered rotation around all axes.[2]

Rebane *et al.* performed polarized Raman measurements on the internal modes of NO_2^- in KCl, KBr, RbCl, and KI in the $\langle 010\rangle\langle 010\rangle$ and $\langle 010\rangle\langle 001\rangle$ polarization geometries.[10] They observed that the $\nu_3(B_1)$ mode in KI did not show any scattered intensity in the I_{yy} setup (consistent with a BT 15 or $q=0$) in contrast with KCl, KBr, and RbCl. This distinct behavior, however, was not attributed to a different orientation of the molecular axis, but the suggestion was made that the differences in polarization properties were all due to the one-dimensional rotation around the O—O axis. The $I_{xy,x\bar{y}}$ intensity was not measured, so that the additional striking differences for the A_1 modes (Figs. 1–3 and Table I) were not revealed.

The polarized Raman data of the NO_2^- in KCl and KBr, presented in this paper, are explained by taking into account both aspects: (a) The BT analysis of the polarized Raman data reveals a threefold axis, and (b) the axial behavior reflects the rotational motion of the ion around the O—O axis.

Evidence for these statements is obtained from the Raman study of the rotational behavior of molecular impurities by Callender and Pershan.[23] They showed that a freely rotating molecule is characterized by a high-frequency spectrum, consisting of a *totally polarized* line at the frequency of the internal vibrational A_1 mode, and a weak depolarized sideband structure, characterizing the rotational dynamics. The KCl:CN^- system, which is at low temperature tunneling between potential wells along the $\langle 111\rangle$ directions,[24] has relatively low barriers to free rotation, as was evidenced by the fact that the room-temperature Raman data are very similar to those expected for a free rotor: The stretching mode is characterized by zero intensities $I_{x\bar{y},z}$ and $I_{xy,x\bar{y}}$. This is expressed in BT parameters as $s/q=0$ and $r/q=1$, i.e., a BT 13, which corresponds to an A_1 mode of the *cubic* group.[18] Due to the three-dimensional rotational motion, the derived polarizability tensor of the stretching mode of the diatomic molecule exhibits *spherical* behavior, i.e., the Raman tensor possesses the diagonal form with $xx=yy=zz$. One can give an analogous interpretation for the axial behavior of the NO_2^- in KCl and KBr at lower temperatures. The one-dimensional quasifree rotation of the ion about the O—O axis along the $\langle 111\rangle$ direction is reflected in the Raman data through the equality of two of the three diagonal components of the Raman tensor. The originally three independent diagonal elements of the orthorhombic system are thus reduced to only two, which corresponds to *axial* behavior of the derived polarizability *around the rotation axis.* Therefore one expects a BT corresponding to an A_1 mode of the C_{3v} point group, i.e., a BT 39.

The Raman data cannot distinguish which axis is the rotation axis, lying along $\langle 111\rangle$. The O—O axis seems the most obvious candidate in view of (a) its large rotational constant (10 times larger than for the dipole axis and the normal on the molecular plane), (b) the evidence from the rotational fine structure on ir and uv absorption, and (c) the existence of analogous molecular defects with similar dynamics (see Sec. IV D).

D. Comparable molecular defects

It is interesting to compare the site symmetry of the NO_2^- ion to those of NO_2 and CO_2^- as derived from electron spin resonance (EPR) data. Two different configurations of the NO_2 molecule have been detected in several alkali halides.[25] One was established to be frozen into $\langle 110\rangle$ planes of the lattice, with its dipole axis along a $\langle 100\rangle$ direction (cf. NO_2^- in KI and NaBr). In the other configuration the O—O axis lies along a $\langle 111\rangle$ direction and the molecule performs a rapid rotation around that axis (cf. NO_2^- in KCl and KBr). This was concluded from the axial symmetry of the g and A tensors with respect to the $\langle 111\rangle$ directions.

Recently, the isoelectronic CO_2^- in KCl was shown to exhibit similar dynamical behavior as the $NO_2\{111\}$.[26] The same rapid rotational motion about the O—O axis along $\langle 111\rangle$ was revealed. In order to study CO_2^-, we x-irradiated KCl:KCO_3 samples, following the production procedures mentioned in Ref. 26. Strong luminescence inhibited the detection of any Raman signal.

V. CONCENTRATION EFFECTS

The polarized Raman spectra of the internal modes in KI with 1.8 mol% KNO_2 and KBr with 1.4 mol% KNO_2 exhibit different features compared to those recorded in KI and KBr with much lower nitrite concentrations (Table II). The spectra are explicitly shown for two NO_2^- concentrations in KI (Figs. 3 and 7). The higher doping levels result in a breakdown of several equalities between polarized Raman intensities, which hold for *randomly* oriented defects in *cubic* lattices.[18] In Table II it is shown that in the highly concentrated samples $I_{xy,z}$ and $I_{x\bar{y},z}$ are no longer equal. In $\{100\}$-cut samples the equality between I_{xz} and I_{yz} still holds, but a clearly different value is found for I_{xy}.

Moreover, the foregoing concentration effects are accompanied by changes in the polarized Raman intensities, which indicate a symmetry lowering: Zero intensities observed in lowly doped samples become nonzero in

the 1.4–1.8 mol % doped samples. A clear illustration is the $\nu_3(B_1)$ mode, which exhibits a nonzero $I_{xy,x\bar{y}}$ intensity in the 1.8 mol % doped KI (Fig. 7), at variance with the zero intensity in the low concentration sample (Fig. 3). Similar but smaller effects are detected for the $I_{xy,x\bar{y}}$ intensities of the A_1 modes in KBr:NO_2^-.

No attempt was made to estimate quantitatively the concentration effects in KI and KBr, e.g., in order to compare the magnitude of the molecular interactions in the two lattices. The different site symmetry of the NO_2^- in both lattices and the availability of only two concentrations inhibited a systematic investigation.

At higher concentrations the influence of impurity aggregation and intermolecular interactions will also be reflected in the Raman spectra. The presence of dimers, trimers, . . . , etc., is generally revealed in Raman[27] and ir[28] data as weak sidebands on the internal modes. One could attribute the nonzero Raman intensities in the highly doped samples to such (nonresolved) sidebands. However, for randomly distributed aggregates the intensity equality $I_{xy}=I_{xz}$ would not break down.

The effects of electric or elastic interactions among the NO_2^- molecular ions are much harder to estimate. We can assume that the cubic symmetry of the NO_2^- site is conserved. Then the analysis of the data within the framework of the BT method—developed for defects in cubic crystals—remains justified and one deals with a nonrandom distribution of the NO_2^- molecules, due to electric and/or elastic dipole interactions. Additionally, a lower symmetry than the one established for the isolated molecular ion has to be considered. Experimental evidence for such ordering phenomena was reported for OH^- in KCl (Ref. 29) and CN^- in NaCl and KCl.[30] It is also possible that the dipole interactions distort the cubic symmetry on a local scale. In that case the BT analysis, which only applies for defects in cubic lattices, cannot be used.

It would be interesting to investigate the polarized Raman behavior of a mixed molecular crystal, e.g., KCN_xBr_{1-x}, which has been studied over the whole concentration range with a variety of experimental techniques. Any resemblance of extended polarized Raman data for this well-known system with the data of Table II would allow one to link the concentration effects with elastic dipole interactions, partial alignment of elastic dipoles or even glassy behavior,[31,32] and local distortion of the cubic symmetry.[33] Polarized Raman data have been published for the high- and low-frequency region of KCN_xCl_{1-x} (Ref. 34), the high-frequency region of KCN_xBr_{1-x} (Ref. 35), and the low-frequency region of $KCN_{0.5}Br_{0.5}$ (Ref. 36). In all cases the data were limited to the common I_{yy} and I_{yz} intensities.

Already from the presently available data, it is sure that detailed polarized Raman measurements are useful to study interaction effects in mixed molecular crystals.

VI. IN BAND RESONANCES AND GAP MODES

A. KI:NO_2^-

1. Peak positions of the gap modes

The low-frequency region (10–300 cm^{-1}) in KI:NO_2^- shows some impurity-induced modes (see Fig. 5), one of which is localized in the gap between the acoustic and optic phonons. A comparison of the Raman and FIR data of this gap region reveals some spectacular differences. The low-temperature high-resolution (0.015 cm^{-1}) far-ir absorption spectrum shows[5] three gap modes at 70.985, 79.124, and 79.804 cm^{-1}, while the Raman spectrum shows only one gap mode. This Raman gap mode was previously determined at 76 cm^{-1} (Ref. 8) and 77 cm^{-1} (Ref. 37), while we deduced a peak position of 78.8±0.5 cm^{-1}, confirmed by the appearance at *lower* frequency of a plasma line of the Ar^+ laser. Under 514.5-nm excitation this plasma line does occur at 77 cm^{-1}.

2. Character of the gap modes

The BT analysis of the polarized Raman intensities (Table I) yields BT 14 for this mode. When using the site symmetry deduced in Sec. III B 1, this BT is compatible with an A_2 mode of the C_{2v} point group, which characterizes a rotational motion around the dipole axis. It should be mentioned that BT 14 is also compatible with O_h:E_g (see Table VIII of Ref. 18).

Comparison of the peak positions of the gap modes suggests the identification of the Raman gap mode with the intermediate IR mode. However, by using a combined technique of persistent ir spectral holeburning in the bending mode at 804.5 cm^{-1} and the detection of the induced FIR changes with interferometry it has been possible to measure the isotope-shifted peak positions of the FIR gap modes.[6] This revealed that the irreducible representations of the modes are A_1, B_2, and B_1, respectively. Therefore the polarization properties of the Raman (A_2) gap mode provide evidence for the existence of *four* gap modes in KI.

The isotope shifts for two of the three modes correspond to a purely translational behavior, while the intermediate B_2 mode reveals a mixed translational-rotational character. The rotation takes place around the O—O axis.[6] As such, the FIR modes seem to be mainly translational, the Raman mode purely rotational.

3. Orthogonality of Raman and FIR results

A clear orthogonality between the results obtained in Raman scattering and FIR absorption is established. Indeed, the Raman gap mode with its A_2 character is not ir active, and is therefore not expected to appear in the FIR spectrum. But all three of the FIR modes are Raman active according to the selection rules of the C_{2v} point group. However, none of them is detected in the Raman spectrum.

Therefore, Evans and Fitchen suggested a point-impurity model for the NO_2^- in KI, in which the molecular ion is assumed *not* to distort the cubic symmetry of the lattice.[8] They considered parity to remain a good quantum number, and a complete separation between Raman and ir activity was argued, following the even and odd representations of O_h, respectively. The Raman gap mode was interpreted as an E_g mode of the cubic group, which is indeed compatible with BT 14 (see Sec. V A 2).

However, polarized holeburning in the $\nu_2(A_1)$ internal mode[5] induces polarization-dependent changes in the phonon gap, indicating that the transition moments of the gap modes are polarized. Therefore the FIR gap modes reflect noncubic behavior of the NO_2^- ion. This was confirmed by the isotope-shift data of the holeburning experiments[6] indicating that two of the three FIR gap modes correspond to a purely translational motion of the NO_2^- ion, which is not expected for a molecular "point" impurity.

The low-frequency Raman gap modes as seen in the 1.8 mol % doped KI:KNO_2 sample exhibit the same concentration effects as the high-frequency internal modes. As mentioned in Sec. V these effects may reflect an alignment of NO_2^- molecules without any distortion of the cubic environment. In that case it is clear that only modes which are related to the internal symmetry of the molecular ion will be sensitive to this alignment. The other possibility incorporates local distortions of the cubic symmetry and will also have its repercussions on modes which involve mainly nearest-neighbor motions. In this respect the Raman data of gap modes, induced by other molecular impurities, are worth mentioning: For the NCO^- in KBr (Ref. 38) and NO_3^- in KI and KBr (Ref. 39) the Raman-active gap modes possess a BT 40, which corresponds to an E mode of the C_{3v} point group, and not to any mode of the full cubic O_h group.

Therefore we favor the identification of the NO_2^- gap mode in KI with a $C_{2v}(A_2)$ mode rather than an $O_h(E_g)$ mode.

4. *Resonant modes*

The low-frequency region in KI shows in addition modes at 60 and 138 cm^{-1}. The Raman intensities of the 60-cm^{-1} mode (Table I) are compatible with a $C_{2v}:A_1$ mode (BT 60). The 138-cm^{-1} mode has zero $I_{x\bar{y},x\bar{y}}$ and $I_{x\bar{y},z}$ intensities (see Table I) and possesses BT 50 (Table VII of Ref. 18), indicating a $C_{4v}:A_1$ mode. However, the form of the $C_{4v}:A_1$ Raman tensor, i.e., zero off-diagonal and nonzero diagonal elements ($xx=yy$ and $xx\neq zz$), is not compatible with the zero $I_{x\bar{y},x\bar{y}}$ intensity, since the quadratic equation in xx/zz, which is obtained by expressing $I_{x\bar{y},x\bar{y}}$ as a function of the Raman tensor elements, has no real roots. It is possible that accidental relations among the tensor elements (e.g., small off-diagonal elements) yield an observed BT, corresponding to a higher symmetry than the actual one.

B. NaBr:NO_2^-

The I_{yy} and I_{yz} intensities for the NaBr:NO_2^- sample (see Fig. 6) show impurity-related features at 90 and 110 cm^{-1}, and at 90 and 113 cm^{-1}, respectively. In spectra with higher resolution the 110-cm^{-1} signal is also present in the I_{yy} intensity as a shoulder superimposed on the 113-cm^{-1} mode. The gap region in NaBr extends from 105 up to 126 cm^{-1}. Raman data have been published for NaBr:NO_2^- samples with lower optical quality,[8] showing a gap mode at 109 cm^{-1} with the same polarization characteristics as the 113-cm^{-1} mode[40] in Fig. 6.

The similarity between KI and NaBr of the polarized Raman intensities in the high-frequency region suggests that one look for the same analogy in the gap region. The 113-cm^{-1} mode in NaBr, characterized by $s/q=0$, is similar to the 78.8-cm^{-1} mode in KI (see Table I) and is therefore attributed to an A_2 mode of C_{2v}. The 110-cm^{-1} mode is tentatively identified as induced by NO_3^- impurities because (a) relatively strong Raman signals were present at frequencies corresponding to NO_3^- normal modes, (b) the spectra of Evans and Fitchen do not show any depolarized scattering on the low-frequency side of the NO_2^- gap mode, and (c) the depolarization of this mode is compatible with the results in NO_3^--doped KI and KBr, in which the gap modes were identified as E modes of a C_{3v} point group.[39] Measurements on a {110}-polished sample should clarify this and would also allow identification of the depolarized mode at 90 cm^{-1}, probably an A_1 mode of the NO_2^-, in analogy with the KI lattice.

VII. FERMI RESONANCE

The high-frequency Raman spectra of the NO_2^- in KI and KBr (Figs. 1 and 2) show, apart from their specific polarized Raman behavior, a major difference in the 1300-cm^{-1} region, which is much more complicated in KI than in KBr.

The doublet structure with peaks at 1308 and 1316.5 cm^{-1} was explained as a Fermi resonance between the combination mode $\nu_3(B_1)+\nu'$ ($\nu'=60$ cm^{-1}, see Sec. VI A 4) and $\nu_1(A_1)$.[11,12] The combination mode of the $\nu_3(B_1)$ mode at 1252 cm^{-1} and the low-frequency mode at 60 cm^{-1} is indeed to be expected at about 1312 cm^{-1}, which is close to the position of the $\nu_1(A_1)$ mode. The averaged position of the doublet structure is exactly 1312 cm^{-1}. The symmetry restrictions governing the Fermi resonance state that the A_1 representation should be included in the direct product of the representations of all participating modes. In this case the direct product of the combination mode $\nu_3\otimes\nu'$ with the totally-symmetric-stretching mode ν_1 should be considered. Rebane and co-workers assumed the 60-cm^{-1} mode to be a B_1 mode, using the polarized Raman spectra of Evans and Fitchen (Ref. 8). Our Raman results agree quantitatively with those of Ref. 8, but the conclusion about the irreducible representation does not agree with Rebane's. The polarized Raman intensities (see Table I) are compatible with an A_1 mode and *not* a B_1 mode. As such the symmetry conditions for a Fermi resonance with the combination mode $\nu_3+\nu'$ are not fulfilled.

The doublet structure is accompanied by a third satellite at about 1333 cm^{-1}. All three components are characterized by a BT 60 (see Fig. 3), corresponding to $C_{2v}:A_1$ modes, and they exhibit similar concentration effects (see Fig. 7). The combination mode of the $\nu_3(B_1)$ mode and the ir-active B_1 mode at 79.804 cm^{-1} has A_1 character and could be identified with the 1333-cm^{-1} mode. A similar explanation for the 1316.5-cm^{-1} mode as being due to a combination mode of $\nu_3(B_1)$ with any

other low-frequency mode is not compatible with the detected A_1 representation for this high-frequency mode. The fact that the frequency difference between satellites 2 and 3 (16.5 cm^{-1}) is twice the distance within the doublet structure (8.5 cm^{-1}) might be accidental. It should be mentioned that some sideband structure is seen at about 12 cm^{-1} on the high-frequency side of the $\nu_1(A_1)$ mode in NaBr:NO_2^-. It would be interesting to investigate the resemblance of this structure with the triplet structure in KI:NO_2^- for NaBr samples with higher NO_2^- concentration and better optical quality.

VIII. CONCLUSIONS

The distinct dynamical behavior of the molecular impurity NO_2^- in different alkali halides, derived from ir and uv absorption measurements,[2,9] is shown for the first time to be connected with a different orientation of the molecular ion in the cubic alkali-halide crystal. The NO_2^- in KI and NaBr, for which hindered rotational motion about all axes was established, possesses C_{2v} symmetry. The Raman data are consistent with the $\langle 100 \rangle$ direction of the dipole axis and the $\{110\}$ orientation of the molecular plane, as was deduced from ir spectral holeburning experiments. The polarized Raman intensities of the internal vibrational modes in KCl and KBr are compatible with a threefold axis. The axial behavior of the derived polarizability reflects the quasifree rotation of the ion most likely about its O—O axis.

The A_2 character of the Raman mode in the gap region of KI yields evidence for the existence of four different gap modes, three of which are ir active and one Raman active. This orthogonality between Raman and FIR results cannot be explained by considering selection rules, governing Raman and ir activity of a C_{2v} impurity system. The experimental data connect ir activity with translational motion and Raman activity with rotational motion.

The polarized Raman intensities show novel concentration effects in relatively highly nitrite-doped alkali halides (>1 mol %). Within the BT analysis they are interpreted as symmetry lowering and breakdown of the random distribution of the molecules.

The idea of a Fermi resonance between $\nu_3(B_1)+\nu'$ ($\nu'=60$ cm^{-1}) and $\nu_1(A_1)$, suggested to explain the doublet structure at 1312 cm^{-1} in KI,[11] is not compatible with the A_1 character of the 60-cm^{-1} mode.

ACKNOWLEDGMENTS

We wish to thank A. J. Sievers for fruitful discussions and for supplying the samples. This work was supported by the NFWO (Nationaal Fonds voor Wetenschappelijk Onderzoek) and the IIKW (Interuniversitair Instituut voor Kernwetenschappen), to which the authors are greatly indebted. We also thank A. Bouwen for experimental support.

*Present address: Natuurkundig Laboratorium, University of Amsterdam, Valckenierstraat 65, NL-1018 XE Amsterdam, The Netherlands.

[1]H. S. Sack and M. C. Moriarty, Solid State Commun. **3**, 93 (1965).
[2]V. Narayanamurti, W. D. Seward, and R. O. Pohl, Phys. Rev. **148**, 481 (1966).
[3]A. J. Sievers and C. D. Lytle, Phys. Lett. **14**, 271 (1965).
[4]K. F. Renk, Phys. Lett. **14**, 281 (1965).
[5]W. P. Ambrose and A. J. Sievers, Chem. Phys. Lett. **147**, 608 (1988).
[6]W. P. Ambrose and A. J. Sievers, Phys. Rev. B **38**, 10 170 (1988).
[7]T. Timusk and W. Staude, Phys. Rev. Lett. **13**, 373 (1964).
[8]A. R. Evans and D. B. Fitchen, Phys. Rev. B **2**, 1074 (1970).
[9]R. Avarmaa and L. Rebane, Phys. Status Solidi **35**, 107 (1969).
[10]L. A. Rebane, T. Yu. Khal'dre, A. E. Novik, and A. A. Gorokhovskii, Fiz. Tverd. Tela (Leningrad) **15**, 3188 (1973) [Sov. Phys.—Solid State **15**, 2129 (1974)].
[11]T. J. Haldre, L. A. Rebane, A. V. Liapzev, and A. A. Kiselev, Phys. Status Solidi B **70**, 359 (1975).
[12]H. J. Jodl and F. Bolduan, Phys. Status Solidi B **103**, 297 (1981).
[13]H. J. Jodl and W. B. Holzapfel, Chem. Phys. Lett. **55**, 259 (1978).
[14]N. Matsukawa, N. Nagasawa, and G. Kuwabara, J. Phys. Soc. Jpn. **54**, 3168 (1985).
[15]W. P. Ambrose and A. J. Sievers, Phys. Status Solidi B **151**, K97 (1989).
[16]G. Dolling, R. A. Cowley, C. Schittenhelm, and I. M. Thorson, Phys. Rev. **147**, 577 (1966).
[17]L. A. Rebane, G. S. Zavt, and K. E. Haller, Phys. Status Solidi B **81**, 57 (1977).
[18]J. F. Zhou, E. Goovaerts, and D. Schoemaker, Phys. Rev. B **29**, 5509 (1984).
[19]D. A. Long, *Raman Spectroscopy* (McGraw-Hill, New York, 1977).
[20]H. Fleurent, W. Joosen, and D. Schoemaker, Phys. Rev. B **38**, 6257 (1988).
[21]H. Fleurent, W. Joosen, and D. Schoemaker, Phys. Rev. B **39**, 10 409 (1989).
[22]R. Claus, L. Merten, and J. Brandmüller, in *Light Scattering by Phonon Polaritons*, Vol. 75 of *Springer Tracts in Modern Physics*, edited by G. Höhler (Springer, Berlin, 1975).
[23]R. Callender and P. S. Pershan, Phys. Rev. A **2**, 672 (1970).
[24]F. Lüty, Phys. Rev. B **10**, 3677 (1974).
[25]J. R. Brailsford and J. R. Morton, J. Magn. Reson. **1**, 575 (1969).
[26]F. Callens, P. Matthys, and E. Boesman, J. Phys. Chem. Solids **50**, 377 (1989).
[27]D. Durand and F. Lüty, Ferroelectrics **16**, 205 (1977).
[28]S. S. Khatri and A. L. Verma, Phys. Lett. **95A**, 191 (1983).
[29]A. T. Fiory, Phys. Rev. B **4**, 614 (1971).
[30]A. Diaz-Gongora and F. Lüty, Phys. Status Solidi B **86**, 127 (1978).
[31]J. M. Rowe, J. J. Rush, D. G. Hinks, and S. Susman, Phys. Rev. Lett. **43**, 1158 (1979).
[32]J. J. De Yoreo, M. Meissner, R. O. Pohl, J. M. Rowe, J. J. Rush, and S. Susman, Phys. Rev. Lett. **51**, 1050 (1983).
[33]K. H. Michel and J. M. Rowe, Phys. Rev. B **22**, 1417 (1980).

[34]D. Durand and F. Lüty, Ferroelectrics **16**, 205 (1977).
[35]F. Lüty, in *Defects in Insulating Crystals,* edited by V. M. Turkevich and K. K. Shvarts (Springer-Verlag, Berlin, 1981).
[36]J. L. Sauvajol, G. Cohen-Solal, and J. F. Berret, in *Proceedings of the Third International Conference on Phonon Physics and Sixth International Conference on Phonon Scattering in Condensed Matter, Heidelberg, August 1989* (World Scientific, Singapore, in press).
[37]L. A. Rebane, K. E. Khaller, and T. Yu Khal'dre, Fiz. Tverd Tela (Leningrad) **17**, 570 (1975) [Sov. Phys.—Solid State **17**, 362 (1975)].
[38]H. Fleurent (unpublished).
[39]K. Elst, Licentiate thesis, University of Antwerp (UIA), 1989 (unpublished).
[40]A wave-number calibration error in the same sense as for the Raman-active gap mode in Kl:NO_2^- (see Sec. VI A 1) explains the difference.